

# Production of Activated Carbon Electrodes from Sago Waste and its application for an Electrochemical Double-Layer Capacitor

E. Taer<sup>1,\*</sup>, A. Afrianda<sup>1</sup>, Apriwandi<sup>1</sup>, R. Taslim<sup>2</sup>, A. Agustino<sup>1</sup>, Awitdrus<sup>1</sup>, and R. Farma<sup>1</sup>

<sup>1</sup> Department of Physics, University of Riau, 28293 Simpang Baru, Riau, Indonesia

<sup>2</sup> Departement of Industrial Engineering, Islamic State University of Sultan Syarif Kasim, 28293 Simpang Baru, Riau, Indonesia.

\*E-mail: [erman.taer@yahoo.com](mailto:erman.taer@yahoo.com)

Received: 8 June 2018 / Accepted: 27 August 2018 / Published: 1 October 2018

---

Research on the utilization of sago waste as an activated carbon electrode for an electrochemical double-layer capacitor (EDLC) has been successfully performed. An important part of the EDLC is the highly porous activated carbon electrode that is prepared without the addition of adhesive materials with an optimum physical activation time. The sago waste-based activated carbon was prepared without adhesive materials with different physical activation times of 0.5, 1.0, 1.5, 2.0 and 2.5 hours. The effect of the physical activation time is discussed in terms of the physical and electrochemical properties of the carbon electrodes. The evaluated physical properties of the electrode include the density, surface morphology, chemical element content, degree of crystallinity and surface area. The electrochemical properties of the supercapacitor cells were studied for specific capacitances on a two-electrode system using the cyclic voltammetry method. The optimum specific capacitance of the sample electrode was  $132 \text{ F g}^{-1}$ , which was achieved with an activation time of 2.5 hours.

---

**Keywords:** sago waste; physical activation time; supercapacitor

## 1. INTRODUCTION

Sago (*Metroxylon* sp.) is an indigenous plant in Indonesia, which has an area of approximately 1.128 million hectares of sago, representing 51.3% of the world's sago. Every year, Indonesia exports 200000 to 260000 tons of sago [1]. The processing of sago flour produces solid and liquid waste. The solid waste is generated from the squeezing process of sago stems which consist of pith fibers. The processing of sago produces a waste of 75-83% [2], and this waste contains 21% lignin, 20% cellulose, extractive substances and ashes [3]. Sago waste is still limited to a few simple uses such as animal feed

[4], weed control [5] and plant fertilizers. The content of lignin and cellulose is high enough so that it is very possible to use sago waste as activated carbon [6]. Sago waste is one of the categories of materials used to produce activated carbon for supercapacitor applications because it has a surface area as high as  $1737 \text{ m}^2 \text{ g}^{-1}$  by a simple activation process [7]. Supercapacitor is an energy storage device that is currently being developed by researchers [8]. In previous studies, the utilization of sago waste as a carbon electrode was carried out by Aripin et al. in 2010 [9] and Afrianda et al., in 2018 [10]. Aripin's samples were prepared by two different activation methods. The first method was a chemical activation process consisting of KOH and carbon with ratios of 1: 1, 2: 1, 3: 1 and 4: 1, followed by carbonization at high temperatures (500–900 °C). The second method was a two-step physical activation process with carbonization at a low temperature of 700 °C, followed by a physical activation at a higher temperature of 800-1000 °C. The activated carbon electrode was prepared using polytetrafluoroethylene (PTFE) as an adhesive material. Aripin's study obtained a specific capacitance of  $64 \text{ F g}^{-1}$ . Afrianda's samples were prepared with a one-stage carbonization and activation process. The samples were activated using KOH as a chemical activation agent and water steam as a physical activation agent. A physical activation time of 1.5 hours was used, which was relatively low. The carbon electrode was prepared without the addition of an adhesive material. A specific capacitance of  $74 \text{ F g}^{-1}$  was obtained for the supercapacitor cell. In this study, sago waste was processed into an activated carbon electrode for supercapacitor applications without adhesive materials with longer physical activation time of 0.5, 1, 1.5, 2 and 2.5 hours. The highest specific capacitance obtained in this study was  $132 \text{ F g}^{-1}$ , which was achieved with a physical activation time of 2.5 hours.

## 2. MATERIAL AND METHODS

### 2.1. Preparation of the carbon electrode

The activated carbon electrode was prepared from sago waste (Dregs Sago) collected in the Selat panjang area, Riau province of Indonesia. Activated carbon was prepared by previously reported methods [11]. Chemical activation was performed using a KOH activator agent at a concentration of 0.2 M. The process of carbonization and physical activation was performed in one stage [12]. The carbonization process was carried out at a temperature of 600 °C for 2 hours under a  $\text{N}_2$  atmosphere, followed by a physical activation at a temperature of 850 °C in a water steam environment. The water steam was maintained for various activation time of 0.5, 1, 1.5, 2 and 2.5 hours. The samples are labeled DS-0.5, DS-1.0, DS-1.5, DS-2.0 and DS-2.5, respectively, where DS refers to dregs sago and the number refers to the activation time. Lastly, all samples were polished and washed until the water became neutral [13]. The processing of sago waste become carbon electrode was shown in Figure 1.

### 2.2. Cell fabrication and electrochemical characteristics

Supercapacitor cells were fabricated in a sandwich type consisting of activated carbon electrodes, separators, current collectors, and electrolyte [14]. In this study, the separator was an

eggshell membrane that has been previously reported [15]. The current collectors were a 316 L stainless steel tape purchased from Goodfellow Cambridge Ltd., England. An aqueous electrolyte was selected as the electrolyte for supercapacitor cells, i.e.,  $\text{H}_2\text{SO}_4$  with a concentration of 1 M purchased from Germany [16].

### 2.3. Physical and electrochemical characteristics

The physical and electrochemical properties were characterized for the activated carbon electrodes. The studied physical properties of the carbon electrode include the density, surface morphology, chemical composition, degree of crystallinity and surface area. The densities were obtained by measuring the mass and the volume. The surface morphology was examined by scanning electron microscopy (SEM). The SEM magnifications used were 5000 and 40000 times. The chemical composition was measured using energy dispersive X-ray (EDX). Measurements of the surface morphology and the chemical composition of the samples through SEM and EDX methods were performed with a JEOL JSM-6510 LA instrument. The degree of crystallinity was measured by X-ray diffraction method (XRD) using a Philip X-Pert Pro PW 3060/10 instrument with a Cu  $k\text{-}\alpha$  light source and a wavelength of 1.5418 Å. The surface area was analyzed using  $\text{N}_2$  adsorption-desorption isotherms with a Quantachrome NovaWin Version 11.0 instrument. The electrochemical properties, i.e., the specific capacitance of the supercapacitor cell, were studied using cyclic voltammetry (CV) method with a Physic CV UR Rad-Er 5841 instrument, which has been calibrated with a 1280 Solartron device. The specific capacitance was evaluated by a standard formula [17,18].



**Figure 1.** Processing of sago waste became the carbon electrode

## 3. RESULTS AND DISCUSSION

### 3.1. Density analysis

The density analysis was performed by measuring the mass and the volume before and after the pyrolysis. Table 1 shows the mass, volume and density before and after the pyrolysis. Based on the data shown in Table 1, the physical activation time has a very significant effect on the mass, volume and density of the carbon electrode. In general, the mass, volume and density decrease with increasing physical activation time. The sample mass decreases regularly with increasing activation time, while the volume also decreases but not as regularly. The increasing activation time results in a smaller density. The density decrease occurred in a range of 13.91-21.82%.

**Table 1.** The mass, volume and density before and after pyrolysis

Sample Codes	Before Pyrolysis			After Pyrolysis		
	Mass (g)	Volume (cm <sup>3</sup> )	Density (g cm <sup>-3</sup> )	Mass (g)	Volume (cm <sup>3</sup> )	Density (g cm <sup>-3</sup> )
DS-0.5	0.654	0.629	1.042	0.243	0.271	0.899
DS-1.0	0.663	0.641	1.037	0.241	0.272	0.889
DS-1.5	0.656	0.628	1.046	0.224	0.264	0.850
DS-2.0	0.651	0.624	1.044	0.222	0.268	0.834
DS-2.5	0.626	0.598	1.048	0.219	0.275	0.799

The largest decrease in the mass, volume and density occurred in the DS-2.5 samples. The DS-2.5 sample has a longer reaction between H<sub>2</sub>O, an activation agent, and the carbon material in the electrode sample, which breaks more carbon chains and causes an optimal evaporation of the impurities, thus leading to more pores and a lower density [19]. This case is similar to the carbon electrode made from rubber wood sawdust with the density range of 0.780-0.587 g cm<sup>-3</sup> [14]. This analysis indicates that 2.5 hours is the optimum physical activation time to produce the best electrode sample.

### 3.2. Analysis of the capacitive properties

The electrochemical properties were measured using cyclic voltammetry (CV) method, and the CV data is shown in Figure 2. Figure 2.a shows the charge-discharge current in a potential window of 0-0.5 V at a scan rate of 1 mV s<sup>-1</sup>. The I-V data for a typical type of carbon electrode material is a rectangular shape [20]. This area indicates that the charge/discharge response for the samples is almost purely electrostatic without a pseudocapacitive phenomenon. The curve area formed represents the specific capacitance produced by the carbon electrode [21].

The charging process begins when the potential is relatively low on the CV instrument, and the electrolyte ions rapidly charge in to the pores of the electrode, so the current density increases significantly. The ion charging process continues until the maximum potential is reached. After this process is complete, the CV instrument starts the discharging process, where the electrolyte ions simultaneously discharge from the pores of the carbon electrode and the current density decreased significantly. The ion discharging continues until the initial potential is reached. A greater I-V area of the electrodes with a higher specific capacitance was produced by a longer physical activation time [22]. Specific capacitances obtained in this study were 29.21 F g<sup>-1</sup>, 48.12 F g<sup>-1</sup>, 90.96 F g<sup>-1</sup> and 132.09 F g<sup>-1</sup> for the DS-0.5, DS-1.0, DS-1.5, DS-2.0 and DS-2.5 samples, respectively. The maximum capacitance produced was higher than that produced with the same base material in Aripin's and Afrianda's studies, which were 64 F g<sup>-1</sup> and 74 F g<sup>-1</sup>, respectively. The highest specific capacitance obtained from this study is almost the same as the specific capacitance generated from the different biomass which shown in Table 2. Figure 2.b shows that the physical activation time affects the capacitive properties of the supercapacitor at a scan rate of 1 mV s<sup>-1</sup>. Increasing the activation time causes a longer reaction between the carbon and the activation agent. This reaction causes more carbon

chains to break and produces more pores. Increasing the pores of the carbon electrode increases the porosity and the surface area of the sample. As a result, the ion diffusion into the pores increases, and the specific capacitance will be higher.

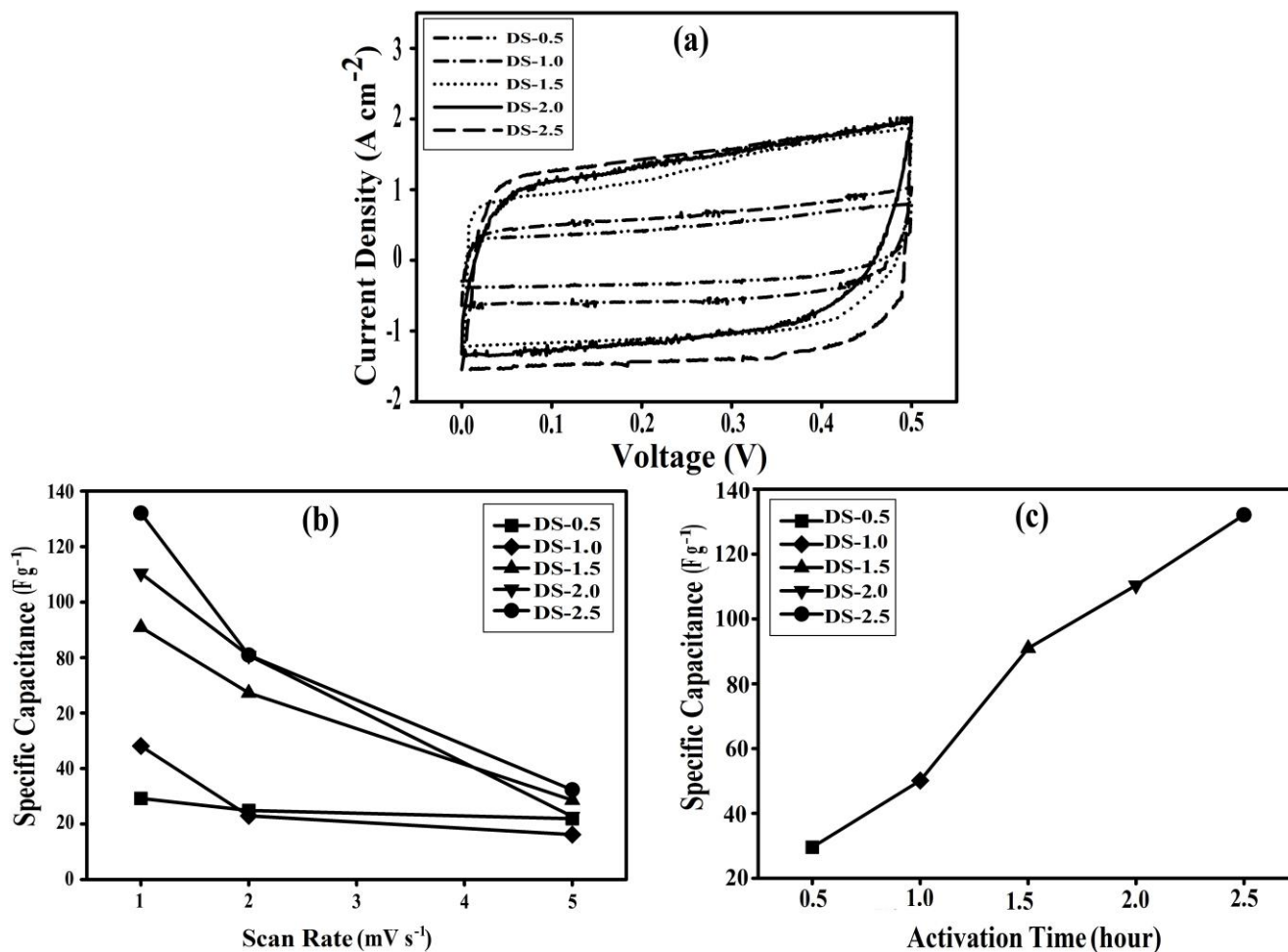


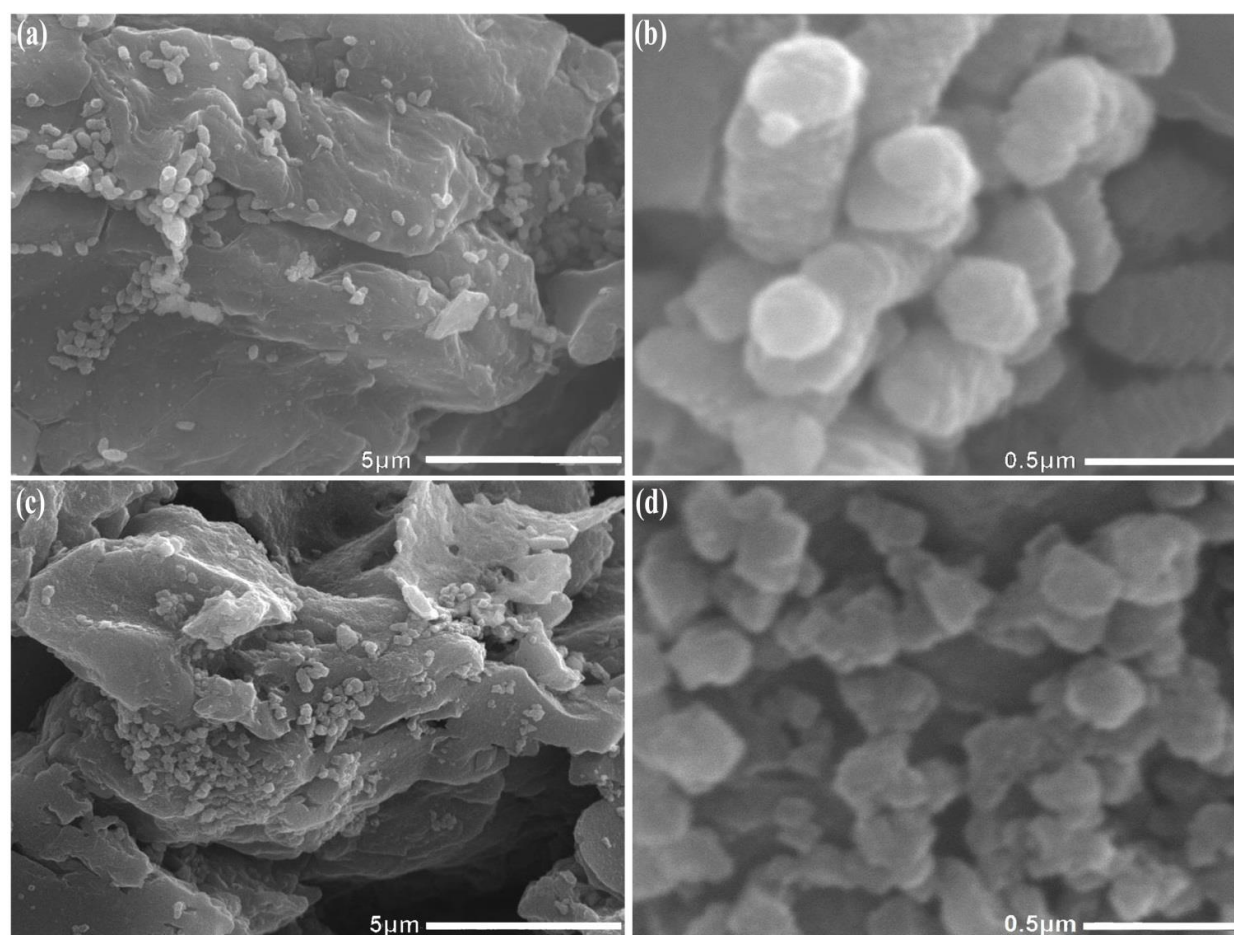
**Figure 2.** a) CV curves for all samples; b) the effect of the physical activation time on the capacitive properties; c) the specific capacitance (F g<sup>-1</sup>) vs the scanning rate (mV s<sup>-1</sup>) for different supercapacitor cells.

The effect of the scan rate on the specific capacitance is also analyzed and shown in Figure 2.c. The scan rates used are 1 mV s<sup>-1</sup>, 2 mV s<sup>-1</sup> and 5 mV s<sup>-1</sup>. The increasing scan rate affects the specific capacitance of all samples. A higher scan rate results in a shorter time for the electrolyte ions to seep into the pores of the carbon electrode, thus resulting in a smaller specific capacitance. Increasing the activation time causes the carbon particles to split into smaller parts, which indicates that the electrodes are produced with smaller and narrower carbon pores [23]. An activation time of 0.5 hours produces a large pore size, and the electrolyte ions easily seep into the pores of the carbon electrode, so the variation of the scanning rate has no effect. A higher activation time results in smaller pore sizes, and the ions take longer to seep into the pores of the carbon electrode. The specific capacitance decreases significantly with increasing scan rate.

**Table 2.** Specific capacitance from different biomass materials

Biomass materials	Specific capacitance ( $F g^{-1}$ )	References
Oil palm fruit	85	[24]
Tobacco	148	[25]
Corn stalk	140	[26]
Fructose corn syrup	168	[27]
Onion	200	[28]
Cattail	126.5	[29]
Banana stem	170	[30]
Rubber wood sawdust	138	[14]
Cow dung	124	[31]
Sago	132	Present study

### 3.3. Analysis of the surface morphology

**Figure 3.** SEM micrographs for a) DS-1.5 with a magnification of 5000 times; b) DS-1.5 with a magnification of 40000 times; c) DS-2.5 with a magnification of 5000 times; d) DS-2.5 with a magnification of 40000 times.

SEM micrographs for the DS 1.5 and DS-2.5 samples with magnifications of 5000 and 40000 times are shown in Figure 3. The SEM micrographs show uneven macropores that exist between the particles with a pore size in the range of 1.3-5.53  $\mu\text{m}$ . The pores formed appear to be an elongated and irregular shape. There are lumps of small carbon particles on the surface of the carbon electrode. The sizes of the carbon particles formed are large, in the range of 0.24-0.5  $\mu\text{m}$ . The sizes of the particles and the pores formed are smaller than the particles in the previously reported sample.

The surface morphology is influenced by the activation time, and a longer activation time causes the particle and the pore sizes to decrease. Increased activation time causes a longer reaction between carbon and steam, thus breaking more carbon chains. Breaking the carbon chain results in cracks and fragments, which forms smaller particles. In addition, increased activation time also causes a faster particle movement, resulting in more particle collisions, which causes the carbon particles to split into smaller parts [23].

#### 3.4. Analysis of the chemical composition

The chemical composition of the sample was measured using the energy dispersive X-ray (EDX) method. The results of the EDX spectra showing the chemical composition of the DS-1.5 and DS-2.5 samples are shown in Figure 4 and Table 3. Table 3 shows that the chemical composition of the sample is dominated by the carbon element (C). In addition to carbon, there are also other elements, such as oxygen (O), magnesium (Mg), potassium (K) and calcium (Ca). The presence of the oxygen element as the second highest composition is due to the carbonization process when the oxygen content in the sample electrode is not completely decomposed. Ca, which is one of the chemical contents in sago waste, has a high boiling point of 1484  $^{\circ}\text{C}$ , so it does not decompose during the process of carbonization and physical activation. The Mg element probably comes from the steel balls that collide with the sample during the smoothing process. The presence of the K element comes from the chemical compound KOH, an activator agent, because the water is not perfectly neutral during the process of washing the sample. The carbon quantity in the DS-2.5 sample is 97.13%, greater than that in the DS-1.5 sample, which is only 89.99%. Increased activation time causes more contents of the elements other than carbon to decompose, so the carbon element produced was higher. The carbon content obtained in this study is also similar to the previously reported carbon content with different carbon materials, such as 98.35% from durian [19] and 87.86% from banana stem [32].

**Table 3.** The chemical composition of the DS-1.5 and DS-2.5 samples

Components	DS-1.5		DS-2.5	
	Mass %	Atom %	Mass %	Atom %
C	85.45	89.99	94.42	97.13
O	11.34	8.96	2.35	1.81
Mg	0.17	0.09	0.25	0.13
K	-	-	1.11	0.35
Ca	3.04	0.96	1.87	0.58
Totals	100%			

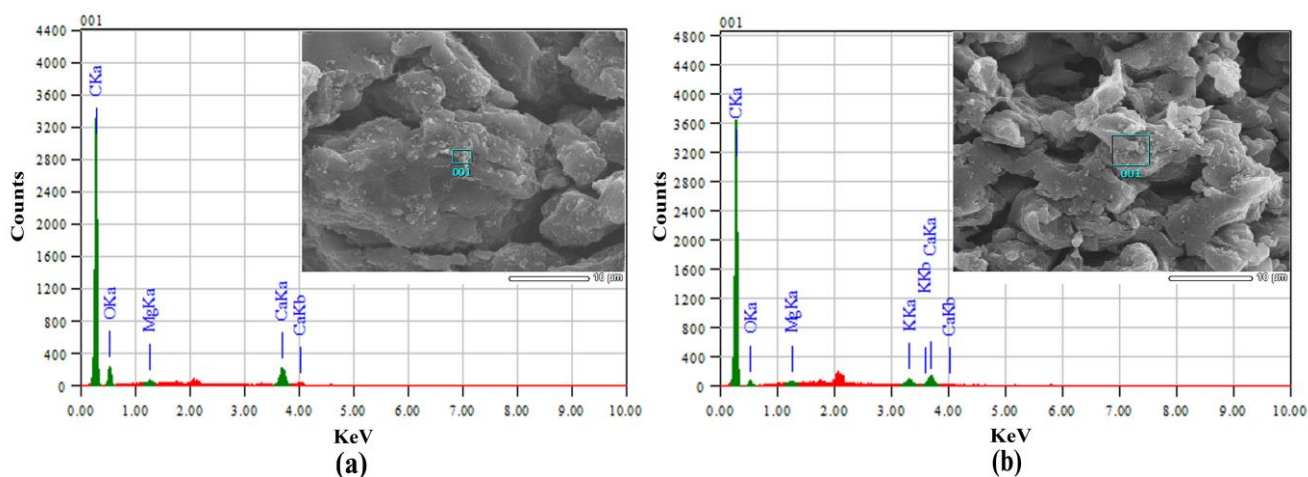


**Figure 4.** The EDX spectra of the DS-1.5 and DS-2.5 samples

3.5. Analysis of the X-ray diffraction, crystallite dimension and surface area

X-ray diffraction analysis (XRD) was performed to determine the nature of the crystallinity in the carbon electrode. The diffraction  $2\theta$  angles used are in the range of  $10^\circ - 100^\circ$ . Figure 5 shows the XRD patterns for the DS-1.5 and DS-2.5 samples, which exhibit a broadening peak shape, indicating an amorphous structure for carbon materials from biomass materials [33]. The  $2\theta$  angles of the 002 and 100 reflection planes for the DS-1.5 sample are  $24.649^\circ$  and  $44.420^\circ$ , respectively, while the  $2\theta$  angles of the 002 and 100 reflection planes for the DS-2.5 sample are  $24.746^\circ$  and  $44.052^\circ$ , respectively. These data suggest that the samples have a good peak coverage for carbon materials [14]. The composition of the carbon structure is also indicated by a  $2\theta$  angle of  $84.107^\circ$  for the 112 reflection plane. Elements and compounds other than carbon are also found in the X-ray diffraction results, as evidenced by the presence of sharp and narrow peaks in the X-ray diffraction pattern. The peaks shown on the DS-1.5 sample curve are from  $\text{CaCO}_3$ , whereas the peaks shown in the DS-2.5 sample are from CO and  $\text{CaCO}_3$ .

**Table 4.** The interlayer spacing and the microcrystallite of the DS-1.5 and DS-2.5 samples

Sample Codes	$2\theta_{(002)}$ ( $^\circ$ )	$2\theta_{(100)}$ ( $^\circ$ )	$d_{(002)}$ ( $\text{Å}$ )	$d_{(100)}$ ( $\text{Å}$ )	$L_c$ ( $\text{Å}$ )	$L_a$ ( $\text{Å}$ )
DS-1.5	24.694	44.420	3.602364	2.037818	11.82018	24.02344
DS-2.5	24.746	44.052	3.594912	2.053984	10.79225	41.77059

Increased activation time resulted in different interlayer spacings and microcrystallite dimensions, as shown in Table 4. The interlayer spacing ( $d_{hkl}$ ) is calculated using the Bragg equation, i.e., [34]

$$n\lambda = 2d \sin 2\theta \tag{1}$$

The microcrystallite dimensions, such as the steak height ( $L_c$ ) and the steak width ( $L_a$ ), are calculated using the following equations [35, 36, 37, 38]:

$$L_a = 1.94 \lambda / \beta \cos \theta_{(100)} \tag{2}$$

$$L_c = 0.89 \lambda / \beta \cos \theta_{(002)} \tag{3}$$

where  $L_c$  and  $L_a$  are the dimensions of the microcrystallites (Å),  $\lambda$  is the wavelength (Å),  $\beta$  is the bandwidth (degree),  $\theta_{(100)}$  is the diffraction angle in the hkl plane 100 and  $\theta_{(002)}$  is the diffraction angle in the hkl plane 002. Increased physical activation time generally does not have a significant effect.

The microcrystallite dimensions,  $L_c$  and  $L_a$ , in the range of 10.66-12.23 Å are almost identical to those of the activated carbon from other biomass materials, such as durian shell, in the range of 10.58-36.21 Å [19]. These data is still in the data range for activated carbon [14]. The stake height can be used to determine the surface area of the electrode sample using the empirical formula [39]:

$$SSA_{xrd} = 2 / (\rho_{xrd} L_c) \tag{4}$$

where  $\rho_{xrd}$  is the XRD density, which is evaluated using the following equation:

$$\rho_{xrd} = (d_{002}(\text{graphite}) / d_{002}(\text{sample})) \rho(\text{graphite}) \tag{5}$$

where  $d_{002}(\text{graphite})$  and  $\rho(\text{graphite})$  are 0.33354 nm and 2.268 g cm<sup>-3</sup>, respectively [39]. The surface area of the sample electrode is shown in Table 4. As seen in Table 5, the microcrystalline dimensions are strongly associated with the surface area. A small microcrystallite height is required to produce a high surface area of activated carbon. DS-2.5 samples have a high surface area of 880.70 m<sup>2</sup> g<sup>-1</sup>, which is almost the same as the electrode surface area of other materials, such as coffee shell and cassava peel waste, which are 842 m<sup>2</sup> g<sup>-1</sup> [40] and 1352 m<sup>2</sup> g<sup>-1</sup> [41], respectively.

**Table 5.** The surface area from XRD for the DS-1.5 and DS-2.5 samples

Sample code	d <sub>(002)</sub> (Å)	L <sub>c</sub> (Å)	ρ <sub>xrd</sub> (g cm <sup>-3</sup> )	SSA <sub>xrd</sub> (m <sup>2</sup> g <sup>-1</sup> )
DS-1.5	3.602364	11.82018	2.0999	805.32
DS-2.5	3.594912	10.79225	2.1042	880.70

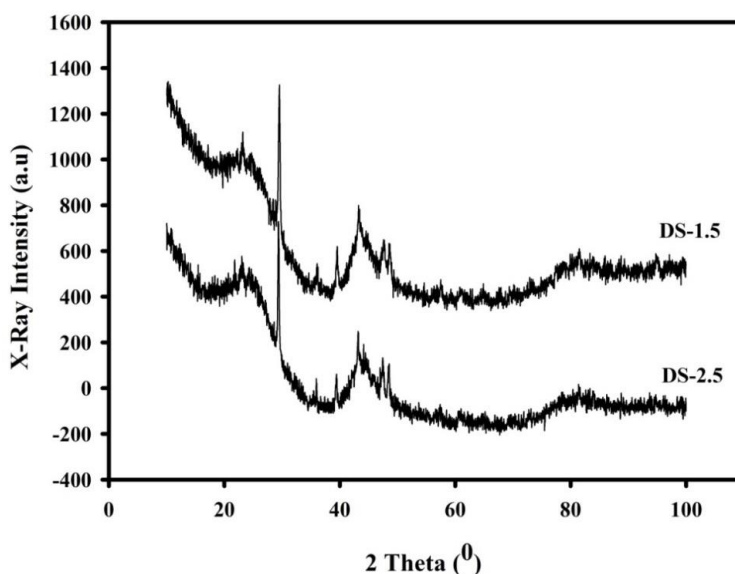


**Figure 5.** The XRD patterns for the DS-1.5 and DS-2.5 samples

The analysis of the physical and electrochemical properties shows interrelated data. The density and the microcrystalline height decrease with increasing physical activation time. Decreasing density and microcrystalline height result in a good porosity, so the surface area of the electrode increases; this is followed by the increase in the carbon content and the capacitive properties of the carbon electrodes. Based on this analysis, it can be concluded that the increase in the physical activation time increases the performance of the electrochemical double-layer capacitor and generates good physical and electrochemical properties.

#### 4. CONCLUSION

Sago waste was found to be one potential candidate as an activated carbon electrode for the electrochemical double-layer capacitor. Sago waste is produced into activated carbon with various physical activation time without the addition of adhesive materials, resulting in good physical and electrochemical properties for EDLC applications. The carbon electrode shows a low density of  $0.799 \text{ g cm}^{-3}$ . The surface morphology shows the formation of small particles and macropores between particles. The carbon content increases with the increase in physical activation time, with the largest carbon as high as 97%. The degree of crystallinity shows that the electrode samples are made from amorphous carbon. The surface area of the sample was evaluated using a standard formula and the microcrystallinity height is  $880 \text{ m}^2 \text{ g}^{-1}$  for the DS-2.5 sample. The analysis of the physical properties is supported by the electrochemical properties, which produce a specific capacitance as high as  $132.09 \text{ F g}^{-1}$  achieved in the sample with a physical activation time of 2.5 hours.

#### ACKNOWLEDGMENTS

The author would like to thank the DRPM Kemenristek-Dikti through the second year Project of PDUPT with the title "Potential of Urban Solid Waste Utilization as a Supercapacitor Electrode" and the contract number: 360/UN.19.5.1.3/PP/2018. The author also thanks the SEM FMIPA ITB Laboratory, which has assisted in obtaining the SEM and EDX data.

#### References

1. Directorate General of Estate Crops, Tree Crop Estate Statistics Of Indonesia 2015-2017 sago. Secretariate of Directorate General of Estate Crops, (2016) jakarta, Indonesia.
2. J. R. Banu, S. Kaliappan, D. Beck, *Water Qual. Res. J. Canada*, 41 (2006) 56.
3. S. Vikineswary, Y. L. Shim, J. J. Thambirajah, N. Blake-Brough, *Resour. Conserv. Recycl.*, 11 (1994) 289.
4. K. Simanihuruk, A. Chaniago, J. Sirait, Sago Waste Silage as Basal Diet for Growing Goats, *Seminar Nasional Teknologi Peternakan dan Veteriner*, Bogor, Indonesia (2011) 542.
5. M. Syakir, M. H. Bintoro, H. Agusta, Hermanto, *Jurnal Littri*, 14 (2008) 107.
6. P. Maheswari, N. Venilamani, S. Madhavakrishnan, P. S. Syed Shabudeen, R. Venckatesh, S. Pattabhi, *J. Chem.*, 5 (2008) 233.

7. I. K. Erabee, A. Ahsan, A. W. Zularisam, S. Idrus, N. N. N. Daud, T. Arunkumar, R. Sathyamurthy, A. E. Al-Rawajfeh, *Engineering Journal*, 21 (2017) 1.
8. A. González, E. Goikolea, J. A. Barrena, R. Mysyk, *Renewable and Sustainable Energy Reviews*, 58 (2016) 1189.
9. H. Aripin, L. Lestari, D. Ismail, S. Sabchevski, *The Open Materials Science Journal*, 4 (2010) 117.
10. A. Afrianda, E. Taer, R. Taslim, *Jurnal Komunikasi Fisika Indonesia*, 14 (2018) 1119.
11. E. Taer, R. Taslim, *AIP Conf. Proc.*, 1927 (2018) 020004-1.
12. E. Taer, Apriwandi, Yusriwandi, W. S. Mustika, Zulkifli, R. Taslim, Sugianto, B. Kurniasih, Agustino, P. Dewi, *AIP Conf. Proc.*, 1927 (2018) 030036-1.
13. E. Taer, M. Deraman, R. Taslim, Iwantono, *AIP Conf. Proc.*, 1554 (2013) 33.
14. E. Taer, M. Deraman, I. A. Talib, A. Awitdrus, S. A. Hashmi, *Int. J. Electrochem. Si.*, 6 (2011) 3301.
15. E. Taer, Sugianto, M. A. Sumantre, R. Taslim, Iwantono, D. Dahlan, M. Deraman, *Adv. Mater. Research*, 896 (2014) 66.
16. Iwantono, E. Taer, A. A. Umar, *AIP Conf. Proc.*, 1454 (2012) 251.
17. S. Faraji, F. N. Ani, *Renew. Sust. Energ. Rev.*, 42 (2015) 823.
18. L. Q. Mai, A. Minhas-Khan, X. C. Tian, K. M. Hercule, Y. L. Zhao, X. Lin, X. Xu, *Nat. Commun.*, 4 (2013) 1.
19. E. Taer, M. Deraman, I. A. Talib, A. A. Umar, M. Oyama, R. M. Yunus, *Current Appl. Phys.*, 10 (2010) 1071.
20. Lee, S. Yi, S. J. Park, *J. Solid State Chem.*, 207 (2013) 158.
21. E. J. Ra, E. Raymundo-Piñero, Y. H. Lee, F. Béguin, *Carbon*, 47 (2009) 84.
22. R. Farma, M. Deraman, A. Awitdrus, I. A. Talib, E. Taer, J. G. Manjunatha, M. M. shak, B. N. M. Dollah, S. A. Hashmi, N. H. Basri, *Bioresource Technol.*, 132 (2013) 254.
23. E. Taer, P. Dewi, Sugianto, R. Syech, R. Taslim, Salomo, Y. Susanti, A. Purnama, Apriwandi, Agustino, R. N. Setiadi, *AIP Conf. Proc.*, 1927 (2018) 030026-1.
24. R. Farma, M. Deraman, Awitdrus, I. A. Talib, R. Omar, J. G. Manjunatha, M. M. Ishak, N. H. Basri, N. M. Dolah, *Int. J. Electrochem. Sci.*, 8 (2013) 257.
25. H. Chen, Y. Guo, F. Wang, G. Wang, P. Qi, X. Guo, B. Dai, F. Yu, *New carbon mater.*, 32, (2017) 592.
26. K. Yu, H. Zhu, H. Qi, C. Liang, *Diamond & Related Mater.*, 88 (2018) 18.
27. W. Cao, F. Yang, *Mater. Today Energy*, 9 (2018) 406.
28. W. Zhang, J. Xu, D. X. Hou, J. Yin, D. B. Liu, Y. P. He, H. B. Lin, *J. Colloid and Interface Science*, 530 (2018) 338.
29. M. Yu, Y. Han, J. Li, L. Wang, *Chem. Engineering Journal*, 317 (2017) 493.
30. E. Taer, R. Taslim, W. S. Mustika, B. Kurniasih, Agustino, A. Afrianda, Apriwandi, *Int. J. Electrochem. Sci.*, 13 (2018) 8428.
31. D. Bhattacharjya, J-S. Yu, *J. Power Sources*, 262 (2014) 224.
32. E. Taer, Y. Susanti, Awitdrus, Sugianto, R. Taslim, R. N. Setiadi, S. Bahri, Agustino, P. Dewi, B. Kurniasih, *AIP Conf. Proc.*, 1927 (2018) 030016-1.
33. G. Yu, L. Lei, J. Yuming, W. Yu, Y. Chuanjun, W. Yingjin, C. Gang, G. Junjie, L. Haiyan, *Appl. Energy*, 153 (2015) 41.
34. F. Li, W. Chi, Z. Shen, Y. Wu, Y. Liu, H. Liu, *Fuel Process Technol.*, 91 (2010) 17.
35. P. J. M. Carrott, J. M. V. Nabais, M. M. L. R. Carrott, J. A. Pajares, *Carbon*, 39 (2001) 1543.
36. B. D. Cullity, *Elements of X-Ray Diffraction*, Ed. 3, (2001) Amazon Prentice Hall.
37. Awitdrus, M. Deraman, I. A. Talib, R. Omar, M.H. Jumali, E. Taer, M. H. Saman, *Sains Malaysiana*, 39 (2010) 83.
38. J. M. V. Nabais, J. G. Teixeira, I. Almeida, *Bioresource Technol.*, 102 (2010) 2781.

39. M. Deraman, R. Daik, S. Soltaninejad, N. S. M. Nor, Awitdrus, R. Farma, N. F. Mamat, N. H. Basri, M. A. R. Othman, *Adv. Mater. Research*, 1108 (2015) 1.
40. M. R. Jisha, Y. J. Hwang, J. S. Shin, K. S. Nahm, T. P. Kumar, K. Karthikeyan, N. Dhanikaivelu, D. Kalpana, N. G. Renganathan, A. M. Stephan, *Mater. Chem. and Phys.*, 115 (2009) 33.
41. A. E. Ismanto, S. Wang, F. E. Soetaredjo, S. Ismadji, *Bioresource Technol.*, 101 (2010) 3534.

© 2018 The Authors. Published by ESG ([www.electrochemsci.org](http://www.electrochemsci.org)). This article is an open access article distributed under the terms and conditions of the Creative Commons Attribution license (<http://creativecommons.org/licenses/by/4.0/>).